

Chiral melting of the Si(113) (3×1) reconstruction

D. L. Abernathy, S. Song, K. I. Blum, R. J. Birgeneau, and S. G. J. Mochrie

*Department of Physics and Research Laboratory of Electronics,
Massachusetts Institute of Technology, Cambridge, Massachusetts 02139-4307*

(Received 23 August 1993)

The results of an x-ray-scattering study of the (3×1)-to-disordered phase transformation of the Si(113) surface are reported. A continuous commensurate-solid to incommensurate-fluid transformation at $T_c = 950 \pm 40$ K is observed. At the transformation, the reconstructed layer becomes uniaxially incommensurate along the cubic (110) direction (x direction). It remains commensurate along the (33 $\bar{2}$) direction (y direction). Critical scattering shows power-law behavior over nearly two decades of reduced temperature [$t = (T - T_c)/T_c$] with exponents $\bar{\beta} = 0.66 \pm 0.05$ for the incommensurability (ϵ), $\nu_x = 0.65 \pm 0.07$ for the inverse correlation length in the incommensurate direction (κ_x), $\nu_y = 1.06 \pm 0.07$ for the inverse correlation length in the commensurate direction (κ_y), and $\gamma = 1.56 \pm 0.13$ for the susceptibility (χ). Below T_c the variation of the square of the order parameter, proportional to the peak intensity at the commensurate position (I_0), varies with an exponent $2\beta = 0.22 \pm 0.04$. It is noteworthy that the correlation lengths in the disordered phase scale anisotropically, that is, $\nu_x \neq \nu_y$, and that the collected exponents do not conform to those of any previously known universality class. In addition to the critical exponents of the transformation, two universal constants have been measured. The ratio of the incommensurability and the inverse correlation length along the incommensurate direction in the disordered phase is found to be independent of temperature, i.e., $\bar{\beta} = \nu_x$, consistent with predictions for a two-dimensional *chiral melting* universality class, and to have the value $w_0 = 1.6 \pm 0.2$. Also, the combination $R_s = \chi\kappa_x\kappa_y/I_0V_r$, where V_r is the two-dimensional resolution volume, is independent of the reduced temperature, consistent with the derived hyperscaling relationship $\nu_x + \nu_y = \gamma + 2\beta$. R_s may be interpreted as the ratio of the integrated intensity of the central part of the critical scattering above T_c ($\chi\kappa_x\kappa_y$) to the integrated intensity of the order parameter scattering below T_c (I_0V_r). According to the hypothesis of two-scale-factor universality, R_s is a universal constant, which we find takes the value $R_s = 0.07 \pm 0.03$.

I. INTRODUCTION

According to the concept of universality, the critical behavior near a continuous phase transformation depends only on the most general aspects of the system in question, such as the symmetry of the phases involved and the dimensionality of space. Thus, the phase transformations of many disparate materials fall into universality classes, within each of which the critical exponents and certain universal constants are independent of microscopic details and delineate the universality class. It is generally believed that two-dimensional (2D) phase transformations may be understood in terms of a limited number of well-known universality classes.¹ Therefore, the appearance of a new 2D universality class is of special interest, particularly when the critical behavior corresponds to a simple and generic statistical mechanical model, and also is unusual in its own right. The experimental characterization of such a universality class is the topic of the present paper.

Transformations between the different phases of a uniaxial overlayer on a substrate allow 2D critical behavior to be studied experimentally. Thus, the commensurate-solid-to-commensurate-fluid transformation of a p -fold commensurate structure [(p ×1) structure] is predicted to be in the universality class of the 2D p -state Potts model,^{2,3} the continuous transformation from a 2D incommensurate (IC) solid to a disordered fluid phase is predicted to be in the Kosterlitz-Thouless (KT) univer-

sality class,⁴ and the commensurate-solid (C-solid) to IC-solid transformation is predicted to lie in the Pokrovsky-Talapov (PT) universality class.⁵ For the transformation from a C solid to an IC fluid, the order of the commensurability (p) is key in determining the expected behavior. It is generally agreed that the continuous disordering of a (2×1) structure ($p = 2$) is inevitably in the universality class of the 2D two-state Potts model, which is equivalent to the 2D Ising model. For $p > 3$, excluding first-order phase transformations, there is agreement that an IC-solid phase separates the C-solid and IC-fluid phases, so that disordering proceeds via successive PT and KT transformations. A realization of C-solid disordering via two transformations, first to an IC-solid and then to a fluid phase, is provided by bromine layers intercalated into graphite, which form a sevenfold commensurate structure at lower temperatures.⁶⁻⁸

In contrast, a transformation that is *not* at present understood theoretically, and offers the possibility of realizing a new universality class, is the disordering of a (3×1) C solid ($p = 3$).^{1,9-14} Figure 1 illustrates generic phase diagrams that have been proposed for the disordering of a (3×1) overlayer. At the special point on the disordering line where light and heavy domain walls (discommensurations) have equal free energies (P), this transformation is in the three-state Potts universality class.¹⁵ Away from P , three competing candidate scenarios have emerged from different treatments of the three-state *chiral* Potts model,^{16,17} which on the basis of universality

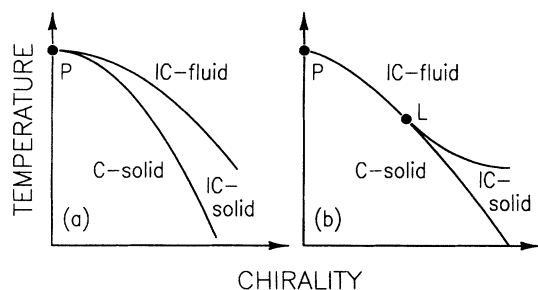


FIG. 1. Proposed phase diagrams of the disordering of a (3×1) overlayer, as described in the text.

is expected to reproduce the critical behavior of a (3×1) overlayer. In contrast to Potts models, for chiral Potts models a domain wall at which the phase of the order parameter changes in a clockwise sense (light domain wall) has a different free energy than a domain wall at which the order parameter changes in a counterclockwise sense (heavy domain wall).

The first possibility, proposed by Haldane, Bak, and Bohr⁹ and by Schulz,¹⁰ is that a direct C-solid to IC-fluid transformation cannot occur for any nonzero *chirality*, defined as the difference in free energy between light and heavy discommensurations. Instead, as shown in Fig. 1(a), disordering is a two step process, involving a PT transformation to an IC-solid phase and, at a higher temperature, a KT transformation to a fluid phase.^{9,10}

The second possibility, sketched in Fig. 1(b) and favored by den Nijs and co-workers^{1,11} and Howes,¹² is that at small chirality there is a direct C-solid-to-IC-fluid transformation in the three-state Potts universality class. This proposal is apparently in contradiction with den Nijs's own determination that the chiral crossover exponent is positive, indicating that chirality is relevant at P .¹⁸ It follows that *a priori* one expects new critical behavior at nonzero chirality. However, den Nijs argues that chirality is a redundant operator, and does not change the critical behavior.¹⁸ Only when the chirality differs significantly from its value at P is the three-state Potts C-solid-to-IC-fluid transformation replaced by successive PT and KT transformations.¹ The multicritical point in the phase diagram where C-solid, IC-solid, and IC-fluid phases meet is called a Lifshitz point (L).

Finally, Huse and Fisher have proposed that, between P and L in Fig. 1(b), the C-solid-to-IC-fluid transformation belongs to a new *chiral melting* universality class.^{13,14} The signature of chiral melting is that the product of the incommensurability and the correlation length approaches a constant near the critical temperature (T_c), that is $\bar{\beta} = \nu$, where $\bar{\beta}$ and ν are the critical exponents for the incommensurability and the inverse correlation length, respectively. In contrast, den Nijs expects $\bar{\beta} = 2\nu$,¹ as found in the exactly solved "hard hexagon" model,¹⁵ which is in the three-state Potts universality class. The product of the incommensurability and the correlation length would in this case go to zero upon approaching T_c . Not surprisingly, since its existence remains a matter of debate, there are no generally accepted values of the critical exponents for chiral melting.

In contrast, the universality classes involved in the first two scenarios are well understood and the corresponding critical exponents are known exactly.

To distinguish among these different theoretical possibilities, one may turn to numerical studies. There seems to be a consensus based on Monte Carlo,^{19,20} finite-size transfer-matrix scaling,²¹⁻²⁵ and Monte Carlo renormalization-group²⁶ calculations that there is a Lifshitz point at nonzero chirality. However, no definitive conclusions can be drawn concerning the critical behavior of the C-solid-to-IC-fluid transformation or its universality class. Thus, it is clear that experimental studies of the disordering of threefold commensurate overlayers that determine the critical exponents accurately are needed.

In the present paper, we report the results of a high-resolution, synchrotron x-ray-scattering study of the (3×1) -commensurate-to-disordered transformation of the Si(113) surface.²⁷⁻²⁹ For Si(113), the reconstructed surface plays the role of the overlayer, while subsequent layers constitute the substrate. Unfortunately, it is not possible to vary the chirality independently. Instead, it must be inferred from experiment where the disordering of Si(113) lies in the phase diagrams discussed above. Our study of Si(113) was motivated by the low-energy-electron-diffraction (LEED) experiment of Yang *et al.*,²⁸ who suggest that the Si(113) (3×1) -to-disordered transformation provides an example of chiral melting. Using the superior resolution available in synchrotron x-ray-scattering experiments, a more complete and accurate characterization of the critical behavior has been obtained. In particular, the behavior of the correlations along the commensurate direction, which could not be resolved in the LEED experiment, has been measured. Also, the critical exponents are shown to satisfy hyperscaling.

Our detailed results may be summarized as follows. We find that Si(113) undergoes a continuous transformation at $T_c = 950 \pm 40$ K, accompanied by critical scaling over nearly two decades of reduced temperature [$t = (T - T_c)/T_c$] with exponents $\nu_x = 0.65 \pm 0.07$ for the inverse correlation length along the incommensurate direction (κ_x), $\nu_y = 1.06 \pm 0.07$ for the inverse correlation length along the commensurate direction (κ_y), $\bar{\beta} = 0.66 \pm 0.05$ for the incommensurability (ϵ), $\gamma = 1.56 \pm 0.13$ for the susceptibility (χ), all above T_c , and $2\beta = 0.22 \pm 0.04$ for the intensity of the commensurate peak (I_0) below T_c . Remarkably, the correlation length exponent along the incommensurate direction differs from that along the commensurate direction: there is *anisotropic scaling*. Such behavior is very unusual and has not been anticipated by previous experimental work on Si(113) or in the majority of theoretical and numerical discussions of (3×1) disordering. The observation of anisotropic scaling is essential in showing that the critical behavior lies outside of the three-state Potts universality class, or any other previously known universality class.

In addition to the critical exponents of the transformation, two purportedly universal constants have been determined. The ratio of the incommensurability and the inverse correlation length in the disordered phase is independent of temperature, consistent with predictions

for the proposed *chiral melting* universality class, and has the value $w_0 = 1.6 \pm 0.2$. Also, the combination $R_s = \chi\kappa_x\kappa_y/I_0V_r$, where V_r is the two-dimensional resolution volume, is independent of the reduced temperature, consistent with the derived hyperscaling relationship $\nu_x + \nu_y = \gamma + 2\beta$. According to the hypothesis of two-scale-factor universality, R_s is a universal constant, which we find takes the value $R_s = 0.07 \pm 0.03$.

Many other surfaces exhibit (3×1) structures, including, for example, Ge(113),³⁰ Cs/Au(110),³¹ O/Cu(210),³² H/Fe(110),³³ and Cs/Cu(110).³⁴ Universality implies that our results may have wide application in understanding the critical behavior of such systems.

The format of this paper is as follows. Section II details our experimental methods. The results and their analysis in the context of current theoretical ideas are presented in Sec. III. In Sec. IV, we conclude. A summary of our results has appeared previously.³⁵

II. EXPERIMENTAL METHODS

We studied *n*-type (phosphorous doped) silicon wafers oriented to within 0.3° of the (113) direction (0.3° mis-cut), with resistivities in the range of 10–100 Ωcm . Each $30 \times 10 \times 0.5 \text{ mm}^3$ sample was held to electrically isolated molybdenum plates by flexible molybdenum clips. A direct current through the sample provided resistive heating, and also served as a convenient measure of the temperature. The temperature of the wafer was measured independently using an optical pyrometer and also by determining the lattice constant using x-ray diffraction at bulk reflections. Standard tables then give the temperature of the sample for the measured lattice constant.³⁶ These two methods agreed in absolute scale to 30 K, and tracked to within 5 K over the range of temperatures studied: 800 K to 1100 K. By fitting the measured temperature versus the sample current to a polynomial, an interpolation formula for converting the current to temperature was derived. The precision of the relative temperature measurement and control was 0.1 K, while the absolute accuracy of the temperature scale is estimated to be 40 K near the disordering temperature. The heating arrangement was found to be quite stable and reproducible, but it should be noted that there was a temperature gradient along the sample due to conductive heat loss at the electrical contacts. The resultant temperature variation across the illuminated area was estimated to be ~ 1.5 K.

Our ultrahigh-vacuum apparatus,³⁷ with standard surface diagnostics and integrated five-circle x-ray diffractometer,³⁷ has a base pressure of less than 7×10^{-11} Torr with the sample at room temperature, and maintained a pressure of less than 6×10^{-10} Torr throughout the measurements. In fact, for the later measurements, the pressure remained below 2×10^{-10} Torr. Samples were cleaned by rapid heating to 1520 K, annealing at 1520 K for one minute, followed by rapid cooling to 1200 K and subsequent slow cooling to the temperatures of interest.²⁸ At the outset of each experiment, the new sample was held at 1100 K for several hours; then the cleaning procedure described above was car-

ried out two or three times. Subsequently, the cleaning procedure was repeated approximately once every 48 hours. During initial sample cleaning, the pressure remained below 1×10^{-8} Torr. In subsequent cleaning cycles, the pressure remained below 2×10^{-9} Torr. Similar procedures have been found to yield well ordered Si(001), Si(111), and stepped Si surfaces in scanning tunneling microscopy studies,³⁸ and were also employed in Refs. 28 and 39 for studies of the Si(113) surface. Our results for the peak intensities, widths, and positions following different cleaning cycles and at different times are in all cases reproducible. In addition, Auger electron spectroscopy, performed using a single-pass cylindrical mirror analyzer, indicated no measurable surface contamination. As determined by measurements of the specular and near-specular x-ray scattering, the surface morphology following the cleaning procedure consisted of large, flat Si(113) facets several thousands of Ångstroms in size, in spite of the macroscopic miscut.³⁷

Figure 2 shows views looking down on the Si(113) surface. As illustrated in Fig. 2(a), the unreconstructed surface may be envisaged as alternating (111) and (001) microterraces, containing (111)-like atoms each with a single dangling bond and (001)-like atoms each with two dangling bonds, respectively. We use a rectangular coordinate system to describe the surface. Referred to the

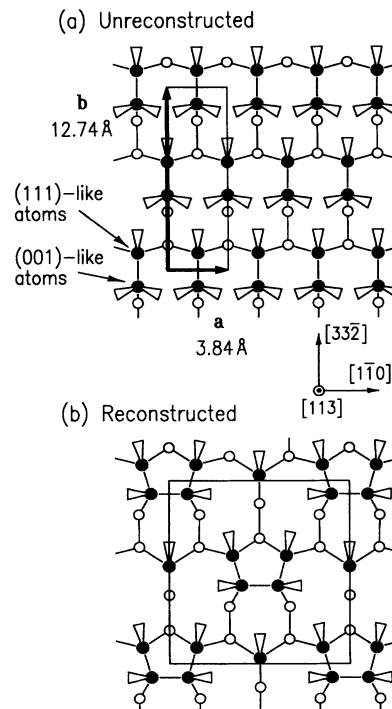


FIG. 2. (a) Top view of an unreconstructed Si(113) surface. The centered, unreconstructed unit cell is outlined, and the rectangular coordinate system used to describe the surface is indicated. Silicon atoms in the surface layer are shown as solid circles. Atoms in lower layers are shown as open circles. Solid lines represent bonds between neighboring atoms, while dangling bonds are shown as triangles. (b) Top view of the Si(113) (3×1) reconstruction. The large box outlines the centered, reconstructed unit cell.

cubic structure of bulk silicon, the surface unit cell vectors defining the x and y axes are $\mathbf{a} = (1, \bar{1}, 0)c/2$ and $\mathbf{b} = (3, 3, \bar{2})c/2$, respectively ($c = 5.43 \text{ \AA}$ at 300 K). With this coordinate system, the unreconstructed Si(113) surface is a centered rectangular structure with 2D lattice constants equal to $a = 3.84 \text{ \AA}$ and $b = 12.74 \text{ \AA}$, as shown in Fig. 2(a). The reconstruction is centered in a cell with the x -axis periodicity tripled. The box in Fig. 2(b) outlines one such cell. A model for the (3×1) reconstruction,³⁹ consistent with measurements of the x-ray structure factor, which are reported elsewhere,³⁷ is depicted in Fig. 2(b). One may imagine that this surface is formed from the unreconstructed surface by removing every third (001)-like atom in the $(1\bar{1}0)$ direction, dimerizing the remaining two (001)-like atoms, and finally re-bonding the (111)-like atom, neighboring the vacancy, to the layer below.

The reciprocal lattice vectors \mathbf{a}^* and \mathbf{b}^* lie along the $[1\bar{1}0]$ and $[33\bar{2}]$ directions in the cubic system, respectively, and have magnitudes of $a^* = 1.64 \text{ \AA}^{-1}$ and $b^* = 0.49 \text{ \AA}^{-1}$. Figure 3 shows the two-dimensional diffraction pattern schematically. Solid squares indicate scattering due to the bulk. Circles represent scattering due to the reconstructed surface at temperatures below T_c , where the reconstruction is found at commensurate, third-order positions along the x axis. Above T_c , the reconstruction becomes incommensurate in the manner indicated by the arrows.

Grazing-incidence x-ray measurements of the surface order and correlations were made at the National Synchrotron Light Source (NSLS). Preparatory experiments

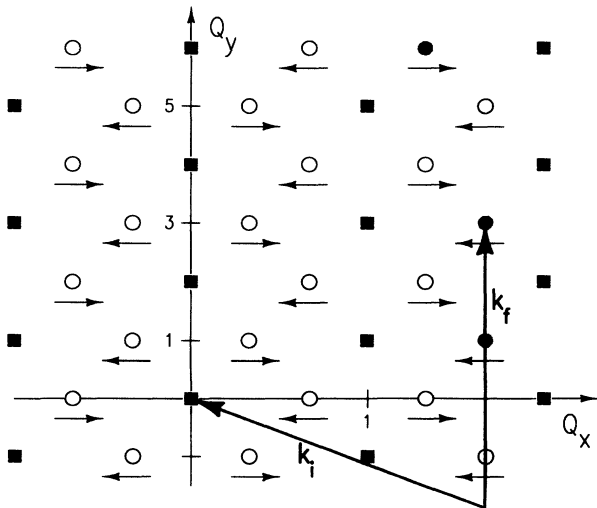


FIG. 3. The diffraction pattern for the Si(113) (3×1) reconstruction. Solid squares indicate scattering due to the bulk, and circles represent scattering from the reconstructed surface. Shaded circles correspond to locations that were investigated in detail, as described in the text. At temperatures below T_c , the reconstruction peaks appear at third-order, commensurate positions. Above T_c , they shift in the directions indicated by the arrows. Also shown is the scattering geometry employed with the linear detector in the second experiment at X25.

were performed at the MIT/IBM X20A bending magnet beamline,⁴⁰ while two separate experiments were carried out at the NSLS X25 wiggler beamline.⁴¹ The first X25 experiment provided an extensive data set, which constitutes the principal basis for our analysis and discussion. The second X25 experiment served to reproduce and confirm our earlier results, under improved vacuum conditions. For the latter experiment, the pressure was less than 2×10^{-10} Torr during measurement.

In brief, beamline X20A focuses synchrotron radiation from a bending magnet using a platinum-coated, bent, cylindrical mirror. A double-crystal monochromator employing Ge(111) reflections selected photons with an energy of 8.8 keV, corresponding to a wavelength of 1.40 \AA . Beamline X25 uses the intense radiation from a 27 pole wiggler, and can be variously configured. For these experiments a double focusing Pt-coated mirror and a Si(111) double-crystal monochromator were used. In the first experiment at X25, photons with an energy of 8.8 keV were also used. The use of X25 led to an improvement in signal by approximately a factor of ten compared to X20A. Measurements were made at a momentum transfer normal to the surface equal to 0.02 \AA^{-1} , giving angles of incidence and exit of $\alpha = 0.2^\circ$.

At X20A and in the first experiment at X25, measurements of the scattering as a function of temperature were made with low- and high-resolution spectrometer configurations. The high-resolution configuration employed a Ge(111) analyzer to define the detector acceptance. A contour plot of the intensity measured at X25 in the C phase at the $(5/3, 1)$ reconstruction peak is shown in Fig. 4(a). At half height the contour is an ellipsoid with major and minor axes (full width) of $\sim 0.0010 \text{ \AA}^{-1} \times 0.0006 \text{ \AA}^{-1}$ in the scattering plane. The high-resolution configuration at X20A also used a Ge(111) analyzer, and was similar to that shown for X25. In the low-resolution configuration, the in-plane angular acceptance of the detector was defined by slits to be 0.3° full width at half maximum (FWHM)

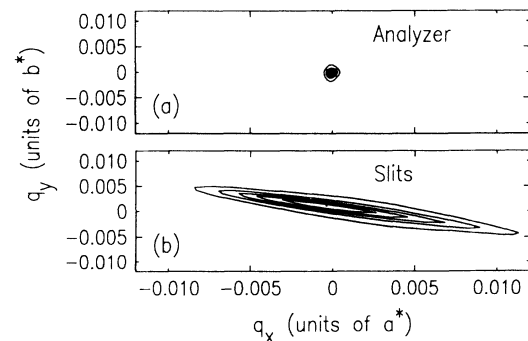


FIG. 4. Contour plots of the intensity of the commensurate $(5/3, 1)$ reconstruction peak at X25. (a) High-resolution configuration employing a Ge(111) analyzer. The half-height contour is an ellipsoid with major and minor axes $\sim 0.0010 \text{ \AA}^{-1} \times 0.0006 \text{ \AA}^{-1}$. (b) Low-resolution configuration using slits to define the exit wave vector acceptance. The half-height contour is an ellipsoid with major and minor axes $\sim 0.016 \text{ \AA}^{-1} \times 0.001 \text{ \AA}^{-1}$.

at X25, so that the half-height contour had dimensions $\sim 0.016 \text{ \AA}^{-1} \times 0.001 \text{ \AA}^{-1}$. Figure 4(b) shows the corresponding contours of the intensity measured at the (5/3,1) peak. It should be noted that for this configuration the direction of the major axis of the resolution ellipsoid varies significantly with position in reciprocal space. This is because the direction of the major axis is always perpendicular to the direction of the scattered wave vector \mathbf{k}_f . At X20A the low-resolution configuration gave roughly the same resolution as at X25.

In the second experiment at X25, in addition to a low-resolution configuration using a conventional point detector, a position-sensitive linear detector was also employed. As will become clear, the form of the critical scattering in Si(113) is highly anisotropic, with the intensity concentrated along lines parallel to the x direction of the surface reciprocal space, motivating the use of a linear detector. Specifically, by suitably choosing the sample geometry and the x-ray energy, it is possible to arrange that the wave vector of the scattered x ray is along the y direction of the surface reciprocal space. It follows that the range of scattering angles accepted by the linear detector corresponds to a line segment in reciprocal space parallel to the x axis. In this way, an entire scattering profile may be collected at one diffractometer setting. The geometry is illustrated in Fig. 3 for the particular case of the (5/3,3) peak, which was the peak studied in the second experiment at X25. For this experiment, it was necessary to choose the x-ray energy to be 6.42 keV. The acceptance out of the scattering plane was defined by slits to be 1.0° in all cases.

III. RESULTS AND DISCUSSION

Below $T_c = 950 \pm 40 \text{ K}$, the Si(113) surface exhibits a threefold commensurate reconstruction along (1,1,0). Figure 5 shows intensity profiles along the x and y directions through the (5/3,1) reconstruction peak at a temperature 5 K below the transformation. These data were obtained using the high-resolution configuration at X25, and are typical for temperatures below T_c . The FWHM for the x and y directions are $0.0006a^* = 0.001 \text{ \AA}^{-1}$, and $0.0012b^* = 0.0006 \text{ \AA}^{-1}$, respectively. The horizontal ranges of both panels in Fig. 5 correspond to 0.013 \AA^{-1} . These widths indicate that the (3×1) reconstruction is well ordered over an area of dimensions at least $6000 \text{ \AA} \times 10,000 \text{ \AA}$ along the x and y directions, respectively.⁴²

Initial studies of the disordering of the Si(113) (3×1) reconstruction were performed at the X20A bending magnet beamline. Figure 6 shows scattering intensities along the x direction through the (-1/3,7) and (1/3,7) reconstruction peaks obtained with a low-resolution configuration for 4 K below T_c (open squares) and 6 K above T_c (filled squares). At the lower temperature, the peaks are at the commensurate positions. At the higher temperature, however, the peaks in the scattering shift from the third-order positions, broaden and weaken dramatically. There is no shift in peak position in the y direction. Measurements at integer-order positions and of the specular and near-specular scattering show no significant changes near T_c , indicating that surface steps play no role in the

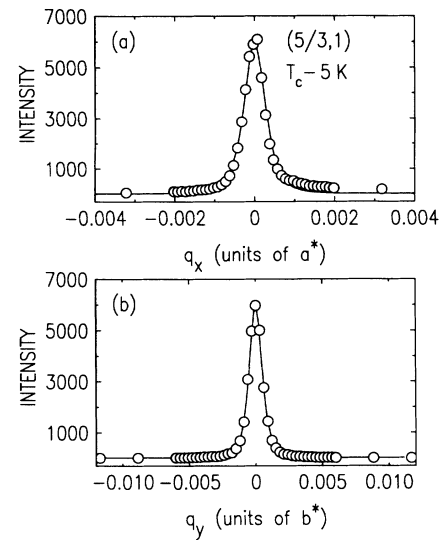


FIG. 5. Scans through the (5/3,1) reconstruction peak along the (a) x and (b) y directions for $T_c - 5 \text{ K}$ obtained at X25 with a high-resolution configuration. The FWHM are (a) $0.0006a^* = 0.001 \text{ \AA}^{-1}$, and (b) $0.0012b^* = 0.0006 \text{ \AA}^{-1}$. The horizontal scales of both panels cover 0.013 \AA^{-1} . Intensity is in arbitrary units.

observed behavior.⁴³

The reconstructed layer has become incommensurate in the x direction only. It follows that in the IC phase the surface is populated by domain walls running on average along the y direction. The FWHM of the IC peak is $\sim 0.02 \text{ \AA}^{-1}$, corresponding to correlated regions of only $\sim 100 \text{ \AA}$ in the x direction at this temperature. The peak shifts shown in Fig. 6 are representative of the alternating pattern of shifts indicated in Fig. 3 by the arrows beneath the reconstruction peak positions. A simple model of the system which incorporates a single type of domain wall or discommensuration shows that this shift will be produced if the registry of the overlayer increases in phase by $+2\pi/3$ upon crossing the domain wall ("light" domain walls).⁴⁴ One may speculate that the row of extra lat-

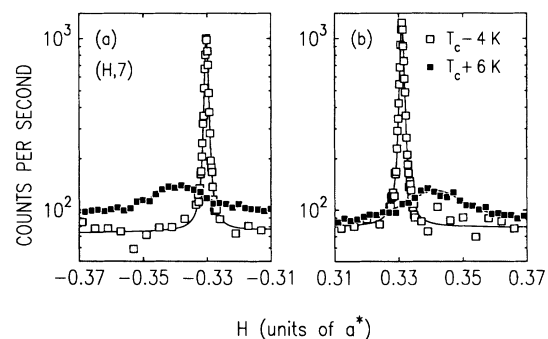


FIG. 6. Scans along the x direction through the (-1/3,7) and (1/3,7) reconstruction peaks obtained at X20 with a low-resolution configuration. At $T_c - 4 \text{ K}$ (open squares), the peaks are commensurate and well ordered. At $T_c + 6 \text{ K}$, the peaks have shifted from the commensurate position and become weaker.

tice units required at each discommensuration between two domains of the threefold surface reconstruction comprises an extra row of rebonded atoms. However, more elaborate wall structures are consistent with the observed shifts as long as the $+2\pi/3$ phase increase is preserved.

In order to study the critical behavior at the disordering transformation over as wide a range of reduced temperatures as possible, it was necessary to employ the high intensity wiggler beamline X25, where we performed detailed measurements of the peak shift, widths, and intensity at the surface $(5/3, 1)$ position. The $(5/3, 1)$ peak was chosen for three reasons: First, the corresponding scattering angle is near the nondispersive condition of the high-resolution configuration, giving the best resolution possible; second, the form of the critical scattering for Si(113) is anisotropic, being much broader along x than along y . At $(5/3, 1)$, the long axis of the low-resolution ellipsoid is quite well matched to the broad direction of the scattering, as may be seen in Fig. 4. The signal is thus maximized without compromising the resolution along y ; third, the structure factor for the $(5/3, 1)$ peak is among the largest.

Figure 7 shows x-ray diffraction profiles versus q_x near $(5/3, 1)$ for several temperatures obtained at the X25 wiggler beamline. At each temperature, the sample was allowed to equilibrate for fifteen minutes before measurement. Below T_c , the scattering profile consists of a narrow peak located at the commensurate position. For temperatures increasing above T_c , the intensity decreases

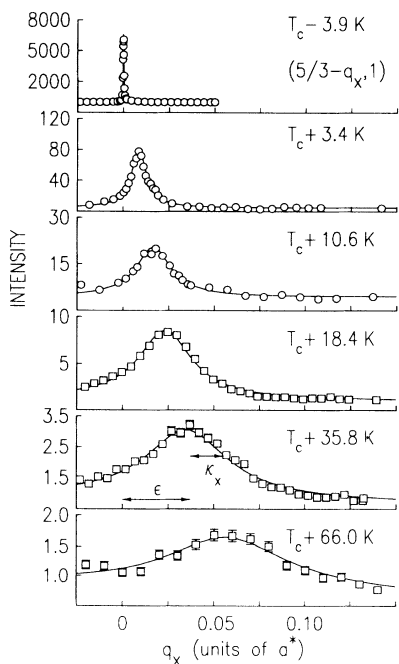


FIG. 7. Scans along the x direction through the peak of the scattering function for various temperatures near $T_c = 959.3$ K obtained at X25. Circles correspond to the high-resolution and squares to the low-resolution diffractometer configuration. The incommensurability (ϵ) and inverse correlation length (κ_x) are indicated graphically. Lines are fits to the Lorentzian form described in the text.

rapidly, while the peak of the scattering shifts away from the commensurate position and its width increases. The three lowest-temperature scans displayed in Fig. 7 were measured with high resolution (circles), while the three highest-temperature scans employed the lower-resolution configuration (squares). Shown in Fig. 8 are the corresponding scans along the y direction, through the peak of the scattering in Fig. 7. Below T_c the peak is narrow, and on heating through the transformation there is an increase in the peak width. However, there is no peak shift in the y direction.

The unidirectional peak shift reflects the formation of uniaxial discommensurations, so that the surface layer is now incommensurate along the x direction, while remaining commensurate in the y direction. The peak broadening indicates that the translational correlation length in the IC phase is finite, so that the IC phase is a fluid. We infer the simultaneous appearance of discommensurations and unpaired dislocations, where three discommensurations meet and end, in the threefold commensurate order at the transformation to the IC phase. The behavior observed here for Si(113) stands in sharp contrast to that seen in bromine-intercalated graphite, for example. Bromine-intercalated graphite constitutes a realization of the seven-state chiral Potts model, and disorders from a sevenfold C solid, as expected theoretically, via two successive transformations, first into an IC-solid phase and then, at higher temperatures, into a fluid phase.⁶⁻⁸ In the IC-solid phase of bromine-intercalated graphite no signif-

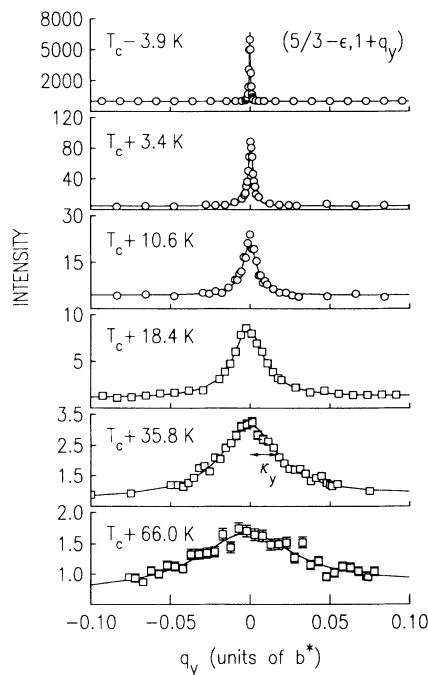


FIG. 8. Scans along the y direction through the peak of the scattering function for various temperatures near $T_c = 959.3$ K obtained at X25. Circles correspond to the high-resolution and squares to the low-resolution configuration. The inverse correlation length (κ_y) is indicated graphically. Lines are fits to the Lorentzian form described in the text.

icant increase in the IC-phase peak width is observed.⁷ This is illustrated in Fig. 9, which shows a direct comparison of the line shapes in the IC phases of Si(113) and bromine-intercalated graphite at similar incommensurabilities. It is apparent, however, that the peak widths are very different for the two cases. Figure 9 demonstrates that IC-solid and IC-fluid phases may be distinguished readily in high-resolution, x-ray-scattering experiments.

To quantify the critical behavior, we fit our measured profiles at each temperature above T_c to a 2D Lorentzian form for the scattering function,

$$S(\mathbf{q}) = \frac{\chi}{1 + (q_x - \epsilon)^2/\kappa_x^2 + q_y^2/\kappa_y^2}, \quad (3.1)$$

where $\mathbf{q} = (q_x, q_y) = \mathbf{Q} - (5/3, 1)$ is the difference between the measured wave vector \mathbf{Q} and the commensurate position. This was convolved with an approximation to the resolution of the instrument. The form used for the resolution in reciprocal space was a Lorentzian squared with an adjustable major axis direction

$$R(\mathbf{q}) = \frac{1}{V_r} (1 + M_{xx}q_x^2 + M_{xy}q_xq_y + M_{yy}q_y^2)^{-2}. \quad (3.2)$$

In Eq. (3.2) the resolution volume V_r is found by requiring that

$$\int R(\mathbf{q})d\mathbf{q} = 1. \quad (3.3)$$

The parameters of the resolutions were determined by fits to the measured scattering in the commensurate phase for the two configurations shown in Fig. 4. On this basis, Eq. (3.2) gives an adequate description of the resolution. Furthermore, Eq. (3.2) allows one integral of the two-dimensional convolution with Eq. (3.1) to be performed analytically, thereby significantly reducing the time required for data analysis. It is important to note that for reduced temperatures greater than about 3×10^{-3} for the high-resolution data and 3×10^{-2} for the low-resolution data, the extent of the resolution function is *much* less than that of the IC-phase scattering function. For larger

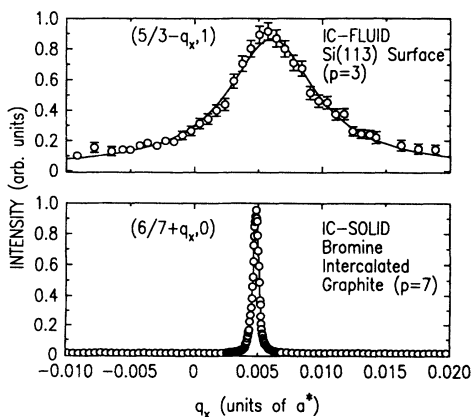


FIG. 9. Comparison of the incommensurate line shapes for an IC-fluid $p = 3$ phase, Si(113), and an IC-solid $p = 7$ phase, bromine-intercalated graphite.

reduced temperatures the resolution contributes at most 10% of width of the experimental profiles.

In addition to the resolution-convolved scattering function, a weakly varying background was added to the model. The form of the background was fixed for all temperatures by the scattering far from the peak. Empirically, the equation

$$I_{bg} = B \left[c + m_x q_x + m_y q_y + \frac{a}{w_x^2 + (q_x - 1/3)^2} \right] \quad (3.4)$$

gave a good description of the observed background. The parameters c , m_x , m_y , a , and w_x were determined at the highest temperature measured using the low-resolution configuration, 1025 K, for which the most extensive data far from the peak of the scattering were available. Subsequent fits varied only the overall background amplitude B , along with the susceptibility χ , the inverse correlation lengths κ_x and κ_y , and the incommensurability ϵ .

Profiles corresponding to the best-fit parameters are displayed in Figs. 7 and 8 as the solid lines. The mean χ squared for all fits in the IC phase was 1.5, with a maximum of 3. Evidently, the 2D Lorentzian gives an excellent description of the data. We note that above T_c , the scattering function for the two-dimensional Ising model has been shown to be very well described by such a form for wave vectors within $\sim 10\kappa$ of the peak.⁴⁵ We have also tried several alternative model line shapes, including line shapes for which the q_x^2 term or the q_y^2 term in the denominator of Eq. (3.1) was replaced by a q_x^3 term or a q_y^3 term, respectively, and a line shape for which a q_x^4 term was added to the denominator of Eq. (3.1). However, as judged by the mean χ squared of fits, these other line shapes provided an inferior description of the experimental profiles.

Below T_c , the scattering consists, in principle, of two components. There is the intensity due to the long-range-ordered reconstruction, and also critical scattering from fluctuations in the ordered state. However, in this experiment we were unable to identify any critical scattering below T_c . We believe it not to be surprising that the critical scattering below T_c was unobservable, for two reasons. First, the intensity of the critical scattering is typically weaker below T_c than above T_c . For the two-dimensional Ising model this factor is 37. Second, because the resolution function is imperfectly known, the strong scattering from the long-range order, which extends away from the nominal commensurate peak position and may overlap the less intense critical scattering, cannot be distinguished from any weak critical scattering.

The commensurate scattering due to the long-range-ordered reconstruction is expected to be a resolution-limited peak with an amplitude proportional to the square of the commensurate order parameter. Thus, to measure the variation with temperature of the order parameter in the C phase, the commensurate peak amplitude (I_0) was found by fits to a Lorentzian-squared function [Eq. (3.2) without the volume normalization V_r], added to the background [Eq. (3.4)]. Examples of the fits are shown as the solid lines in Fig. 5. The order parameter was measured for both the high-resolution and low-resolution configurations. The background for the

low-resolution configuration was 20 times that for the high-resolution data. This simply reflects the change in the two-dimensional resolution volume, as seen in Fig. 4. The peak intensity at a given temperature for the low-resolution data, however, was a factor of 3 higher than for the high-resolution configuration, which we believe is a result of the slight tilt of the rod of scattering with respect to the scattering plane because of the nonzero incidence angle.

An idea essential to our understanding of continuous phase transformations is that in the critical region all quantities of interest vary as a power of the correlation length. As an example, Fig. 10 shows the susceptibility χ and width κ_x versus κ_y . The only adjustment to the fitted values is a multiplication of the intensities obtained in the high-resolution configuration by a factor of 60, consistent with the observations in the C phase discussed above. The overlap for the fit parameters is good where both high- and low-resolution configurations were used, demonstrating that our deconvolution procedures give consistent results. The scaling behavior evident in Fig. 10 indicates that the observed critical behavior may be characterized by a single set of critical exponents. In particular, there is no evidence of any crossover behavior. Accordingly, in our analysis we have used a single power law to describe the behavior of each quantity of interest as a function of the reduced temperature. An advantage of presenting the data as in Fig. 10 is that the exponent is independent of the choice of T_c or of any change in the temperature scales between different experiments.

Figure 11 shows our results for the incommensurability (ϵ), the inverse correlation lengths (κ_x and κ_y), and the susceptibility (χ) versus reduced temperature $t = (T - T_c)/T_c$, obtained in the first experiment at X25. Also shown is the intensity in the C phase (I_0), which is proportional to the square of the order parameter.

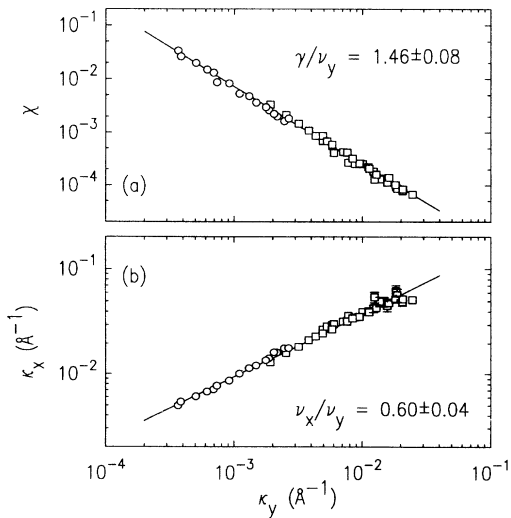


FIG. 10. The susceptibility χ (a) and width κ_x (b) versus the width κ_y . Note the logarithmic scales, indicating power-law behavior for these quantities. Squares are from low-resolution scans, circles from high-resolution data obtained at X25.

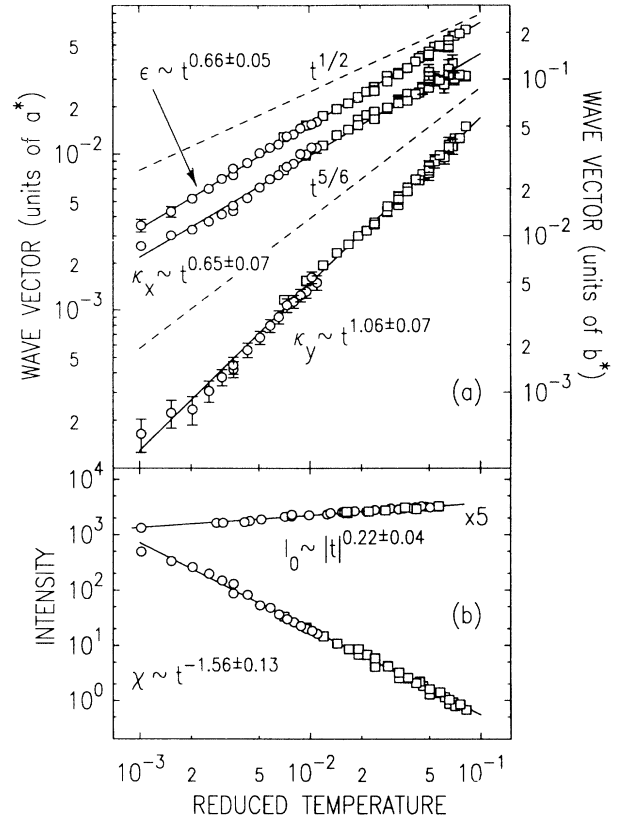


FIG. 11. (a) Incommensurability (ϵ), inverse correlation lengths (κ_x , κ_y), (b) susceptibility (χ), and square of the order parameter (I_0) versus reduced temperature $t = (T - T_c)/T_c$. Circles correspond to the high-resolution and squares to the low-resolution configuration at X25.

The temperature for a given data set was determined using the interpolation formula for converting the sample heating current to a temperature. Intensities for the high-resolution data have been scaled by the factor of 60 as discussed above, and have also been shifted down in temperature by 1 K to match the low-resolution results, for which the nominal transformation temperature was $T_c = 959.3$ K. The high-resolution data set was obtained immediately following the low-resolution set, and each took 48 hours to complete. Both data sets consist of a warming cycle upward through the transition and a subsequent cooling cycle. Within each cycle no hysteresis was observable, so the results for warming and cooling are not distinguished in Fig. 11. The apparent shift in T_c between the high- and low-resolution data sets may reflect a true shift upward in the transformation temperature over time, or it may correspond to a drift in the current-temperature relationship. Another possibility is that the configuration with the analyzer sampled a slightly different region of the surface, with a different apparent T_c .

Each of the quantities plotted in Fig. 11 shows power-law behavior over nearly two decades of reduced temperature with exponents $\beta = 0.66 \pm 0.05$ for the incommensurability, $\nu_x = 0.65 \pm 0.07$ for the inverse correlation length in the x direction, $\nu_y = 1.06 \pm 0.07$ for the inverse

correlation length in the y direction, $\gamma = 1.56 \pm 0.13$ for the susceptibility, and $2\beta = 0.22 \pm 0.04$ for the square of the order parameter. As shown in Fig. 12, for a limited temperature range of ~ 1.5 K around T_c , the measured line shape cannot be described by a single symmetric peak. We attribute the peak asymmetry to a temperature variation across the illuminated sample area. For the same reason, the data used in determining the critical exponents were restricted to reduced temperatures greater than 10^{-3} . The errors in our determination of the exponents derive primarily from our uncertainty in T_c . Specifically, by fixing T_c at the extremes of the possible range of transformation temperatures, and then varying the amplitude and exponent of the power law, the extreme values for the various exponents were found. Table I shows a summary of the amplitudes and exponents so obtained for the power-law fits displayed in Fig. 11. We believe that these exponents are sufficiently accurate that meaningful comparison between experiment and quantitative theory should now be possible.

It is noteworthy that the exponents for the power laws versus reduced temperature are consistent with the exponent ratios found from fits such as those displayed in Fig. 10. For example, fits to the susceptibility χ and x -direction width κ_x versus the y -direction width κ_y give the exponent ratios $\gamma/\nu_y = 1.46 \pm 0.08$ and $\nu_x/\nu_y = 0.60 \pm 0.04$. These are consistent with the ratios of our best determination of the exponents from the reduced temperature power laws, where $\gamma/\nu_y = 1.47$ and $\nu_x/\nu_y = 0.61$. The agreement for other exponent ratios is similar.

Table II compares the values of the incommensurabil-

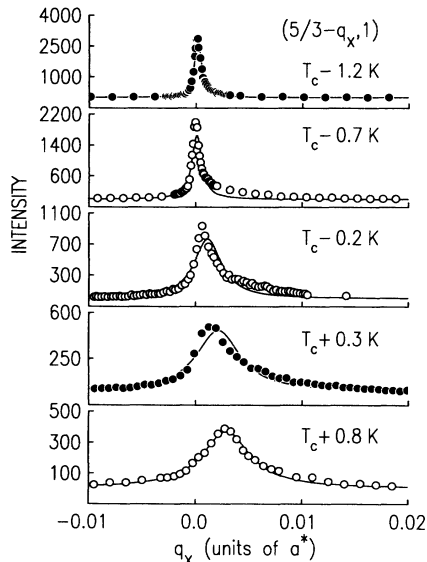


FIG. 12. Scans along the x direction through the peak of the scattering function close to the transformation temperature ($T_c = 959.3$ K) obtained at X25 in the high-resolution configuration. Open circles correspond to warming and filled circles to cooling. Lines are fits to the Lorentzian form described in the text, which for the temperature range $T_c - 0.75$ K $< T < T_c + 0.75$ K do not adequately describe the data.

TABLE I. Amplitudes and exponents of power-law fits.

	Amplitude	Exponent
ϵ	$0.20 \pm 0.03 \text{ \AA}^{-1}$	0.66 ± 0.05
κ_x	$0.12 \pm 0.02 \text{ \AA}^{-1}$	0.65 ± 0.07
κ_y	$0.32 \pm 0.05 \text{ \AA}^{-1}$	1.06 ± 0.07
χ	0.015 ± 0.006	1.56 ± 0.13
I_0	1250 ± 250	0.22 ± 0.04

ity (ϵ) and the two widths (κ_x and κ_y) determined for the lowest and highest temperatures used in fitting the exponents. Also shown are the associated length scales in real space. The correlation lengths (ξ_x and ξ_y) are simply the inverse of the widths, and an upper limit for the mean spacing between discommensurations (l) is given by $l = 2\pi/3\epsilon$.⁴⁶ In the IC phase, the ratio of the correlation length along the x direction and the discommensuration separation is always $\xi_x/l \approx 1$. At the highest temperature studied, 1025 K, the mean separation between discommensurations is estimated to be 22 Å, while the correlation lengths are 16 Å along x and 56 Å along y . It is remarkable that at this temperature both the spacing of discommensurations and the correlation length along the x direction are less than two (3×1) unit cell lengths. The correlation length in the y direction indicates that order is lost within five unit cell lengths in that direction. The high brightness of X25 enables x-ray-scattering measurements of such a disordered surface structure.

The results presented in Figs. 10 and 11 make it clear that the exponent for the correlation length along x differs from that for the correlation length along y . Such anisotropic scaling is very unusual. For example, for the two-dimensional Ising model the correlations scale with the same exponent, even if the interactions are themselves highly anisotropic.⁴⁷ One instance in which anisotropic scaling does occur is the uniaxial C-solid-to-IC-solid transformation, where exact results give $\nu_x = \bar{\beta} = 1/2$ and $\nu_y = 1$.⁵ For comparison, a power law with exponent 1/2 (dashed line) is shown at the top of Fig. 11. It is evident that this exponent is excluded by our measurements of both the incommensurability (ϵ) and the inverse correlation length (κ_x). The only other phase transformation at which anisotropic scaling has been documented experimentally is the transition from a nematic to smectic liquid crystal in three dimensions.⁴⁸

Another possibility to be considered is that the exponents should be those of the three-state Potts model, for which $\nu_x = \nu_y = 5/6$, $\gamma = 13/9$ and $\beta = 1/9$.^{2,3,15} Comparison of our measurements of the peak widths and incommensurability to a power law with exponent 5/6, shown as a dashed line in Fig. 11, demonstrate that the Si(113) disordering transformation cannot be in that universality class.

It is noteworthy that the measured values of the exponents are consistent with hyperscaling. Specifically, a scaling hypothesis for the correlation function near T_c gives rise to the (anisotropic) hyperscaling relation $\nu_x + \nu_y = 2 - \alpha$, where α is the exponent describing the divergence of the specific heat. In addition, a scaling form of the critical free energy leads to the relation

TABLE II. Lengths and wave vectors for the extreme temperatures used in determining the exponents in the IC phase.

T	960.3 K		1025 K	
Reduced temperature t	0.001		0.069	
Incommensurability ϵ	$0.0035a^*$	0.0057 \AA^{-1}	$0.057a^*$	0.093 \AA^{-1}
x width κ_x	$0.0026a^*$	0.0043 \AA^{-1}	$0.038a^*$	0.062 \AA^{-1}
y width κ_y	$0.00055b^*$	0.00027 \AA^{-1}	$0.036b^*$	0.018 \AA^{-1}
Mean wall spacing l	$96a$	370 \AA	$5.8a$	22 \AA
x correlation length ξ_x	$60a$	230 \AA	$4a$	16 \AA
y correlation length ξ_y	$280b$	3600 \AA	$4.4b$	56 \AA

among thermodynamic exponents $\alpha + 2\beta + \gamma = 2$. Thus, one expects $\nu_x + \nu_y - \gamma = 2\beta$, which is satisfied by the measured values. The exponent values also suggest that the specific heat exponent $\alpha = 2 - \gamma - 2\beta = 0.22 \pm 0.17$ may be smaller than the value for the three-state Potts transformation, where $\alpha = 1/3$, although the three-state Potts value is by no means excluded. The possibility of a value for α smaller than $1/3$ was suggested by Huse and Fisher in the context of chiral melting.¹⁴

A more direct test of hyperscaling, independent of the fitted values of the critical exponents, can be made by plotting the dimensionless ratio

$$R_s = \chi \kappa_x \kappa_y / I_0 V_r, \quad (3.5)$$

where V_r is the two-dimensional resolution volume and the other quantities are those shown in Fig. 11. R_s may be interpreted as the ratio of the integrated intensity of the central part of the critical scattering above T_c to integrated intensity of the order parameter scattering below T_c . Figure 13 shows the combination R_s for the subset of our data where the reduced temperature for the determination of the commensurate peak intensity I_0 below T_c matched to within 5% the reduced temperature for a set of χ , κ_x , and κ_y above T_c . It is gratifying that R_s is indeed independent of the reduced temperature, indicating that hyperscaling is satisfied.

In fact, according to the concept of two-scale-factor universality first introduced by Stauffer, Ferer, and Wortis,⁴⁹ the value of R_s is a constant for each universal-

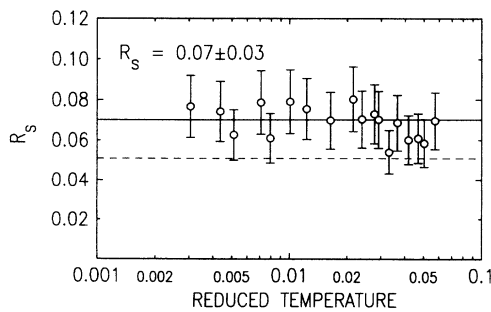


FIG. 13. Plot of $R_s = \chi \kappa_x \kappa_y / I_0 V_r$ versus reduced temperature $t = (T - T_c) / T_c$. R_s is a universal number for each universality class. The theoretical value of R_s for the 2D Ising model (0.051) is shown as the dashed line. The solid line corresponds to our best fit value of $R_s = 0.07 \pm 0.03$ for chiral melting.

ity class. Two-scale-factor universality relates the critical amplitudes near a continuous phase transformation by assuming that the magnitude of the singular part of the free energy within a correlated volume in units of $k_B T_c$ is the same for systems within the same universality class. This result has also been shown to follow from application of the renormalization group.⁵⁰ In the context of scattering experiments, Bruce has demonstrated that Eq. (3.5) embodies the idea of two-scale-factor universality.⁵¹ As seen in Fig. 13, R_s takes the value 0.07 ± 0.03 for the transformation under study. For comparison, the dashed line in Fig. 13 shows the exact value of R_s for the 2D Ising model (0.051). A neutron scattering study of Rb_2CoF_4 measured a value of 0.043 ± 0.002 for that realization of the 2D Ising model.⁵²

Another universal number, specific to the proposed chiral melting transformation,^{13,14} is the product of the incommensurability and the correlation length along the x direction, $\omega_0 = \epsilon / \kappa_x$. To test the hypothesis that the incommensurability and the inverse correlation length scale with the same exponent, one may plot their ratio as a function of the reduced temperature, as shown in Fig. 14. We find that the ratio is independent of reduced temperature, as expected for chiral melting, and takes the value $\omega_0 = 1.6 \pm 0.2$, consistent with the ratio of our best fit amplitudes from Table I. For the one-dimensional three-state chiral Potts model, where an exact solution is possible, the ratio has been determined to be $\omega_0 = \cot(\pi/3) \approx 0.58$, which is shown in Fig. 14 as the dashed line.¹⁴ The larger value of ω_0 found here suggests that in two dimensions correlations are increased

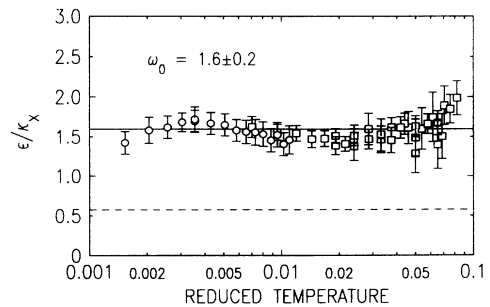


FIG. 14. Product of the incommensurability and the correlation length along the x direction (ϵ / κ_x) versus reduced temperature. The dashed line is the exact result in one dimension (0.58). The solid line is our best fit value of $\omega_0 = \epsilon / \kappa_x = 1.6 \pm 0.2$.

relative to the one-dimensional case. For krypton on graphite, which may be in a different universality class than Si(113) because of its triangular rather than uniaxial symmetry,^{13,14,53} the results of Moncton and co-workers^{54,55} nevertheless indicate that in the hexagonal case ϵ/κ_x also tends to a constant of order one as the reduced temperature goes to zero. The range of reduced temperature over which ϵ/κ_x is constant is, however, much larger for Si(113).

An important check on our results for the critical exponents and universal constants follows from a comparison with the results obtained at X20A and in the second experiment at X25 and with the results of others. Figure 15 shows scans for several temperatures along the x direction near the (4/3,6) reconstruction peak obtained at X20A with a high-resolution diffractometer configuration. The behavior of the scattering on passing through the transformation is very similar to that seen in Fig. 7 for the scattering near (5/3,1) obtained at X25. In particular, the Lorentzian form of the scattering function again provides an excellent description of the data, as shown by the solid lines in Fig. 15. One difference is that for the X20A data our best estimate is that $T_c = 930.6$ K, instead of $T_c = 959.3$ K for the first X25 experiment. In the second experiment at X25, we found $T_c = 962.5$ K. In view of the variation in the observed T_c and the uncertainty in determining the bulk lattice constant, we estimate that the absolute value of the transformation temperature is $T_c = 950 \pm 40$ K. Other investigations of the disordering of the Si(113) reconstruction give transition temperatures in this range. Olshanetsky and Mashanov²⁷ place T_c at 1020 K, and

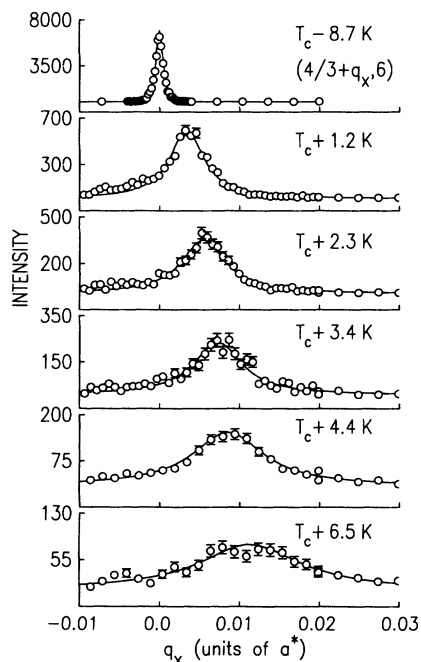


FIG. 15. Scans along the x direction through the peak of the scattering function near (4/3,6) for various temperatures obtained at X20A with a high-resolution diffractometer configuration. In this experiment, we measure $T_c = 930.6$ K. Lines are fits to the Lorentzian form described in the text.

Xing *et al.*⁵⁶ at 870 K. In the detailed study by Yang *et al.*,²⁸ two different experimental runs, carried out in different chambers, yielded transformation temperatures of 844 K and 900 K. Noting the difficulty of absolute temperature measurements of the surface, our transformation temperature is in agreement with these previous experiments.

Figure 16 is a compilation of the incommensurability as a function of the reduced temperature from our various x-ray experiments. The data from X25 using low-resolution (open squares) and high-resolution (open circles) configurations obtained at the (5/3,1) reconstruction peak agree in detail with those from X20A using a high-resolution configuration at the (4/3,6) position (open triangles) and with data from the second X25 run using point detector and linear detector configurations at the (5/3,3) position (open stars). All of the x-ray data agree with the best fit power-law form with an exponent $\bar{\beta} = 0.66 \pm 0.05$, which is shown as a solid line in Fig. 16. Also shown in Fig. 16 are data from the LEED investigation of Yang *et al.*²⁸ (solid circles). It is apparent that the x-ray data are of higher quality, and accordingly yield more precise values for $\bar{\beta}$, as well as for the other critical exponents, than the LEED data.

In Ref. 28, the ratio of the peak shift to its width along the x direction is approximately temperature independent but takes the value ~ 0.8 , in apparent conflict with our result that $w_0 = 1.6 \pm 0.2$. However, for a scattering function which (as we have shown) is well described by a 2D Lorentzian, the relatively broad resolution along q_y employed in Ref. 28 effectively integrates the scattering function over q_y . The resultant measured intensity ver-

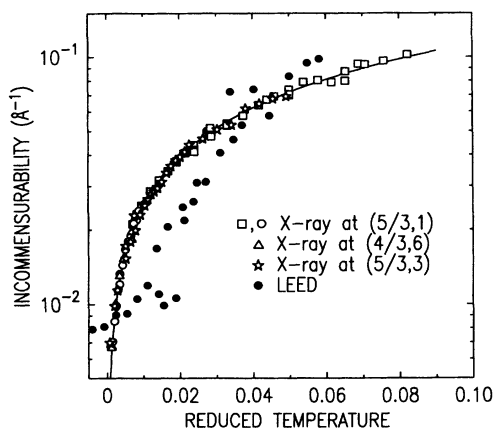


FIG. 16. A comparison of the incommensurability as a function of reduced temperature for several x-ray configurations. Also shown are the previous LEED results (solid circles) of Yang *et al.* (Ref. 28). X-ray data obtained with low resolution (open squares) and high resolution (open circles) at the (5/3,1) reconstruction peak in the first experiment at X25 agree with the high-resolution results obtained at X20 studying the (4/3,6) peak (open triangles), and with the results of the second experiment at X25 using the linear detector (open stars). The solid line corresponds to an exponent for the incommensurability of $\bar{\beta} = 0.66$, as described in the text. To calculate the reduced temperature corresponding to the LEED data the quoted value of $T_c = 844$ K was used.

sus q_x has a half width at half maximum that is increased relative to that of the original Lorentzian scattering function by a factor of $\sqrt{3}$. In other words, the widths given in Ref. 28 should be divided by $\sqrt{3}$ before comparison to our values of κ_x . Likewise, the ratio of the measured peak shift to the measured width should be multiplied by $\sqrt{3}$, yielding a value of $w_0 \sim 1.4$, consistent with our value.

In light of our anomalous results for the critical exponents, it is worthwhile to consider whether surface contamination by a foreign, adsorbed species, albeit at immeasurably small concentrations, might be responsible for the observed critical behavior at the (3×1) -to-disordered transformation of the Si(113) surface. However, certain aspects of our results refute this idea, at least within the context of our current understanding of how random impurities affect critical behavior. First, we note that small concentrations of mobile impurities are not expected to change the universality class of the transformation. Second, we consider immobile adsorbed species that locally favor a particular commensurate sublattice. Such impurities constitute a *random field*.⁵⁷ For 2D Potts models, the effect of a random field is to suppress the disordering temperature to absolute zero. Since we observe a nonzero transformation temperature and a well ordered commensurate phase below 960 K, there can be no random-field impurities on length scales relevant to the present experiment. Third, there may exist immobile impurities that do not distinguish among the commensurate sublattices, but nevertheless attract or repel the domain walls. Impurities of this sort give rise to *random-bond* disorder.⁵⁸ The critical behavior of systems for which the specific heat exponent (α) is negative remains unaffected by random-bond disorder. In systems for which the specific heat exponent is positive in the absence of random-bond disorder, such as the three-state Potts model, the critical behavior is changed to that of the corresponding random-bond universality class. However, for all cases of which we are aware in which the random-bond critical exponents are known, the specific heat exponent is negative. For instance, the specific heat exponent of the random-bond three-state Potts model is negative.⁵⁸ In contrast, on the basis of hyperscaling, we infer a positive specific heat exponent for the (3×1) -to-disordered transformation of Si(113). We therefore believe that a random-bond universality class may also be ruled out.

What are the implications of our results for the proposed phase diagrams of the three-state chiral Potts model? First, we consider the phase diagram of Haldane, Bak, and Bohr⁹ and Schulz.¹⁰ According to these authors, except at the Potts point (P), an IC-solid phase intervenes between the C-solid and the IC-fluid phases, so that there are two successive transformations. However, the temperature range of the IC-solid phase decreases to zero as P is approached. The Si(113) surface is not at the Potts point, since we observe a transformation to an IC phase indicating the preferential formation of discommensurations with a phase shift of $+2\pi/3$ in the commensurate order parameter. We may also rule out an IC-solid phase more than ~ 1 K wide intervening

between the observed C-solid and IC-fluid phases. It follows that if the phase diagram proposed by Haldane, Bak, and Bohr and by Schulz is to be correct, then Si(113) must nevertheless be close to P , so that the magnitude of the chirality is small. However, it is known that at P the chiral crossover exponent ($\phi = 1/6$) is small.¹⁸ Therefore, for small chirality one expects to observe three-state Potts critical scattering over a large temperature range above T_c , followed by a crossover to KT critical behavior very near T_c . In fact, we observe anisotropic scaling throughout the temperature range studied, which seems inconsistent with the anticipated behavior. Moreover, as the temperature is increased within the C-solid phase, according to Haldane, Bak, and Bohr and to Schulz, the system approaches a PT transformation, near which the order parameter is expected to be only weakly temperature dependent.¹⁴ Thus, the observed power-law behavior of the order parameter versus reduced temperature below T_c also seems incompatible with the scenario of Haldane, Bak, and Bohr, and of Schulz. These arguments lead us to believe that the phase diagram proposed by Haldane, Bak, and Bohr and by Schulz is inappropriate for Si(113).

The existence of a direct C-solid-to-IC-fluid transformation *not* in the three-state Potts universality class allows for two alternative interpretations within the context of current theory. The first possibility, suggested by the experimental result that $\bar{\beta} = \nu_x$, is that the C-solid-to-IC-fluid transformation of Si(113) lies in the chiral melting universality class proposed by Huse and Fisher, and that its critical exponents have now been determined. This interpretation finds support in the finite-size-scaling calculations of Vescan, Rittenberg, and von Gehlen, who studied a highly anisotropic chiral three-state Potts model. Their study reveals a C-solid-to-IC-fluid transformation exhibiting anisotropic scaling with exponents ν_x , ν_y , and $\bar{\beta}$ very similar to those observed for Si(113). However, no Lifshitz point and no IC-solid phase emerge from their calculations, irrespective of the chirality.

The second possibility is that the observed critical behavior at the disordering of the Si(113) (3×1) reconstruction is associated with the Lifshitz point. In this regard, it is interesting that our results for ν_x and ν_y are close to the values suggested by Howes for the Lifshitz point based on series expansions of an anisotropic three-state chiral Potts model. Specifically, using thirteenth-order series expansions at the chirality, which he identifies as corresponding to the Lifshitz point, Howes finds that the exponents for the specific heat (α), the order parameter (β), and the susceptibility (γ) take the values of the three-state Potts model, for which $\alpha = 1/3$, $\beta = 1/9$, and $\gamma = 13/9$. Using a ninth-order expansion, he also finds that the correlation length in the y direction scales with an exponent $\nu_y = 1$ at the proposed Lifshitz point. Assuming the hyperscaling relation $2 - \alpha = \nu_x + \nu_y$, these results imply that in the x direction the correlation length exponent ν_x takes the value $2/3$. Moreover, the arguments of Huse and Fisher, which led them to propose a chiral melting universality class, seem also to apply at the Lifshitz point, leading us to expect that $\bar{\beta} = \nu_x$ there as well. However, in a Landau-Ginsburg description, the

Lifshitz point corresponds to the vanishing of the q_x^2 term in the denominator of the scattering function and, therefore, to a non-Lorentzian line shape. In contrast, we find that the scattering function is Lorentzian. Any theory that seeks to locate the disordering transformation of Si(113) at a Lifshitz point should resolve this apparent discrepancy.

Finally, we note that an unphysical, self-dual version of the three-state chiral Potts model is exactly solved at a special point with exponents $\alpha = 1/3$, $\nu_x = 2/3$, and $\nu_y = 1$.^{59–61} However, the relevance of these latter calculations to transformations in two-dimensional layers is unclear. In any case, our experiment provides definitive evidence of a chiral melting universality class with critical exponents that are unambiguously distinct from those of the three-state Potts model. It remains to be established whether such behavior is unique to the Lifshitz point or whether it holds along the line in the phase diagram from P to L .

IV. SUMMARY AND CONCLUSIONS

In this paper, the results of an x-ray-scattering study of the disordering transformation of the Si(113) (3×1) reconstruction surface have been presented. At 950 ± 40 K there is a continuous transformation from a commensurate-solid phase to an incommensurate-fluid phase. Critical scattering shows single-power-law behavior over nearly two decades of reduced temperature ($t = (T - T_c)/T_c$) with exponents $\bar{\beta} = 0.66 \pm 0.05$ for the incommensurability (ϵ), $\nu_x = 0.65 \pm 0.07$ for the inverse correlation length in the incommensurate direction (κ_x), $\nu_y = 1.06 \pm 0.07$ for the inverse correlation length in the commensurate direction (κ_y), and $\gamma = 1.56 \pm 0.13$ for the susceptibility (χ). Below T_c the variation of the square of the order parameter, proportional to the peak intensity at the commensurate position (I_0), varies with an exponent $2\beta = 0.22 \pm 0.04$. It is remarkable that the correlation lengths in the disordered phase scale anisotropically ($\nu_x \neq \nu_y$). The observed critical behavior is inconsistent with that of any previously known universality class, but consistent with the prediction for chiral melting that $\bar{\beta} = \nu_x$. In addition to the critical exponents of the transformation, two universal constants have been measured. The ratio of the incommensurability and the inverse correlation length in the disordered phase is found to be independent of temperature, and to have the value $w_0 = \epsilon/\kappa_x = 1.6 \pm 0.2$. Also, the combination $R_s = \chi\kappa_x\kappa_y/I_0V_r$, where V_r is the two-dimensional resolution volume, is independent of the reduced temperature, consistent with the hyperscaling relationship $\nu_x + \nu_y = \gamma + 2\beta$. According to the hypothesis of two-scale-factor universality, R_s is a universal constant, which we find takes the value $R_s = 0.07 \pm 0.03$. We hope that

these observations will help in guiding new theoretical investigations into the nature of this unusual, and still controversial, transformation.

The results presented here lead one to speculate on further experiments. First, the existence of a new chiral melting universality class should be reflected in the shape of the scattering function. Since this functional form is universal according to the scaling hypothesis, it would be interesting to pursue scattering experiments near T_c with improved temperature uniformity to examine any deviations from the simple Lorentzian form assumed in our analysis. Theoretical guidance on the form of the scattering function at T_c would also be helpful. Second, if another (3×1)-to-disordered transformation can be found, which yields the same quality of data as in the present experiment, an investigation of its critical behavior could possibly provide an example of universality. In fact, recent LEED experiments indicate that the Ge(113) (3×1) surface has a transformation similar to the Si(113) (3×1) surface.³⁰ It is unlikely that Ge(113) has the same chirality as Si(113), so that the observation of the same critical exponents and universal constants in that system would be strong evidence that they are indeed appropriate along a line in the temperature-chirality phase diagram. Alternatively, deviations may indicate that the Si(113) transformation is at a special point.

Finally, this experiment demonstrates that synchrotron x-ray studies of surface phases and 2D phase transformations have progressed to the point that they can now yield data of sufficient precision to identify and characterize convincingly new (as well as previously known) universality classes. Indeed, the data presented in this paper for a single-crystal silicon surface are of comparable or superior quality to synchrotron x-ray-scattering studies of heavy rare gases adsorbed on high-surface-area graphite substrates^{54,55,62} and quasi-two-dimensional intercalation compounds,⁷ and to neutron scattering studies of phase transformations in layered quasi-two-dimensional magnetic systems,^{52,63} which previously have set the standard for measurements of 2D critical behavior.

ACKNOWLEDGMENTS

We thank N. Bartelt, N. Berker, L. Berman, M. den Nijs, M. Fisher, D. Gibbs, R. Holaday, K. Jacobi, R. Johnson, M. Kardar, B. McClain, D. Noh, I. Robinson, P. Siddons, M. Yoon, and D. Zehner for very valuable comments, discussion, and assistance. Work performed at MIT was supported by the JSEP (DAAL-03-92-C-0001). DLA acknowledges IBM for support. KIB was supported in part by the NSF (DMR-9119675). X20A is supported by the NSF (DMR-9022933). The NSL was supported by the DOE (DE-AC0276CH00016).

¹ M. den Nijs, in *Phase Transitions and Critical Phenomena*, edited by C. Domb and J. L. Lebowitz (Academic Press, London, 1988), Vol. 12.

² M. P. M. den Nijs, *J. Phys. A* **12**, 1857 (1979).

³ B. Nienhuis, E. K. Riedel, and M. Schick, *J. Phys. A* **13**, L189 (1980).

⁴ J. M. Kosterlitz and D. J. Thouless, *J. Phys. C* **5**, L124 (1972).

- ⁵ V. L. Pokrovsky and A. L. Talapov, Phys. Rev. Lett. **42**, 65 (1979).
- ⁶ A. Erbil, A. R. Kortan, R. J. Birgeneau, and M. S. Dresselhaus, Phys. Rev. B **28**, 6329 (1983).
- ⁷ S. G. J. Mochrie, A. R. Kortan, R. J. Birgeneau, and P. M. Horn, Z. Phys. B **62**, 79 (1985).
- ⁸ S. G. J. Mochrie, A. R. Kortan, R. J. Birgeneau, and P. M. Horn, Phys. Rev. Lett. **58**, 690 (1987).
- ⁹ F. D. M. Haldane, P. Bak, and T. Bohr, Phys. Rev. B **28**, 2743 (1983).
- ¹⁰ H. J. Schulz, Phys. Rev. B **28**, 2746 (1983).
- ¹¹ S. Howes, L. P. Kadanoff, and M. den Nijs, Nucl. Phys. B **215**, 169 (1983).
- ¹² S.F. Howes, Phys. Rev. B **27**, 1762 (1983).
- ¹³ D.A. Huse and M.E. Fisher, Phys. Rev. Lett. **49**, 793 (1982).
- ¹⁴ D.A. Huse and M.E. Fisher, Phys. Rev. B **29**, 239 (1984).
- ¹⁵ R.J. Baxter and P.A. Pearce, J. Phys. A **15**, 897 (1982).
- ¹⁶ S. Ostlund, Phys. Rev. B **24**, 398 (1981).
- ¹⁷ D.A. Huse, Phys. Rev. B **24**, 5031 (1981).
- ¹⁸ M. den Nijs, J. Phys. A. **17**, L295 (1984).
- ¹⁹ N.C. Bartelt, T.L. Einstein, and L.D. Roelofs, Phys. Rev. B **35**, 4812 (1987).
- ²⁰ W. Selke and J. M. Yeomans, Z. Phys. B **46**, 311 (1982).
- ²¹ W. Kinzel, W. Selke, and K. Binder, Surf. Sci. **121**, 13 (1982).
- ²² W. Kinzel, Phys. Rev. Lett. **51**, 996 (1983).
- ²³ P. M. Duxbury, J. Yeomans, and P. D. Beale, J. Phys. A **17**, 179 (1984).
- ²⁴ J. Yeomans and B. Derrida, J. Phys. A **18**, 2343 (1985).
- ²⁵ T. Vescan, V. Rittenberg, and G. von Gehlen, J. Phys. A. **19**, 1957 (1986).
- ²⁶ J.M. Houlrik and S.J. Knak Jensen, Phys. Rev. B **34**, 325 (1986).
- ²⁷ B.Z. Olshanetsky and V.I. Mashanov, Surf. Sci. **111**, 414 (1981).
- ²⁸ Y.-N. Yang, E. D. Williams, R. L. Park, N. C. Bartelt, and T. L. Einstein, Phys. Rev. Lett. **64**, 2410 (1990).
- ²⁹ Y.-N. Yang, N. C. Bartelt, T. L. Einstein, R. L. Park, and E. D. Williams, in *The Structure of Surfaces III*, edited by K. Takayanagi and X. D. Xie (Springer-Verlag, Berlin, 1991).
- ³⁰ J. Schreiner, W. Selke, and K. Jacobi, in *Proceedings of the 13th General Conference, Condensed Matter Division of the European Physical Society, Regensburg, March 29-April 2, 1993*, Europhysics Conference Abstracts Vol. 17A (Verhandlungen, Berlin, 1993), p. 1555.
- ³¹ P. Häberle, P. Fenter, and T. Gustafsson, Phys. Rev. B **39**, 5810 (1989); G. A. Held, J. L. Jordan-Sweet, P. M. Horn, A. Mak, and R. J. Birgeneau, Solid State Comm. **72**, 37 (1989) observed the reversible disordering of a (3×1) structure of the Au(110) surface with no measurable impurities. Since the clean Au(110) surface is believed to exhibit an equilibrium (2×1) structure, these authors inferred the presence of trace impurities which produced the (3×1) structure found in their study.
- ³² C. S. McKee, L. V. Renny, and M. W. Roberts, Surf. Sci. **75**, 92 (1978).
- ³³ R. Imbihl, R. J. Behm, K. Christmann, G. Ertl, and T. Matsushima, Surf. Sci. **117**, 257 (1982).
- ³⁴ R. Schuster, J.V.Barth, G. Ertl, and R.J. Behm, Phys. Rev. Lett. **69**, 2547 (1992).
- ³⁵ D. L. Abernathy, R. J. Birgeneau, K. I. Blum, and S. G. J. Mochrie, Phys. Rev. Lett. **71**, 750 (1993).
- ³⁶ *Thermal Expansion - Nonmetallic Solids, Thermophysical Properties of Matter*, edited by Y. S. Touloukian, R. K. Kirby, R. E. Taylor, and T. Y. R. Lee (IFI/Plenum, New York, 1977), Vol. 13.
- ³⁷ D. L. Abernathy, Ph.D. thesis, Massachusetts Institute of Technology, Cambridge, Massachusetts, 1993.
- ³⁸ B. S. Swartzentruber, Y.-W. Mo, M. B. Webb, and M. G. Lagally, J. Vac. Sci. Technol. **7**, 2901 (1989).
- ³⁹ The atomic structure of Si(113) at 300 K is discussed in K. Jacobi and U. Myler, Surf. Sci. **284**, 223 (1993), and references therein.
- ⁴⁰ NSLS Handbook, Brookhaven National Laboratory, Upton, NY, 11973 (1990).
- ⁴¹ L. E. Berman, J.B. Hastings, T. Oversluizen, and M. WOODLE, Rev. Sci. Instrum. **63**, 428 (1992).
- ⁴² We relate the FWHM of diffraction maxima associated with finite-size domains to the domain size (L) via $L = 2\sqrt{4\pi \ln 2}/\text{FWHM} = 5.9/\text{FWHM}$; see for example, P. Dutta and S. K. Sinha, Phys. Rev. Lett. **47**, 50 (1981).
- ⁴³ I. K. Robinson, E. Vlieg, and K. Kern, Phys. Rev. Lett. **63**, 2578 (1989). In contrast to the present case, these authors argue that steps are fundamental to the disordering of the (2×1) reconstruction of the Pt(110) surface.
- ⁴⁴ R. A. Cowley, Adv. Phys. **29**, 1 (1980).
- ⁴⁵ C. A. Tracy and B. M. McCoy, Phys. Rev. B **12**, 368 (1975).
- ⁴⁶ For uniformly separated, ideally narrow discommensurations, the incommensurability ϵ is related to the discommensuration separation l by $\epsilon = 2\pi/3l$ for $p = 3$ (Ref. 44). For such a structure there are also satellite peaks displaced from the primary peak by integer multiples of 3ϵ . In particular, there is a satellite peak located at -2ϵ from the commensurate position, with an amplitude smaller by a factor of 4 than that of the peak at $+\epsilon$. In our study we have seen no evidence for such a satellite at the 10^{-2} level, suggesting that the correlations between discommensurations are significantly reduced from those assumed in Ref. 44. It is noteworthy that the exact solution of the one-dimensional, three-state chiral clock model in the low-temperature limit, which does not show a -2ϵ satellite, relates the mean discommensuration separation to the incommensurability via $\epsilon = \sin(2\pi/3)/l$ (Ref. 14), which is also equal to the center of mass of the scattering of the perfectly ordered discommensuration structure. We infer that $l = 2\pi/3\epsilon$ provides an upper bound on the discommensuration separation l .
- ⁴⁷ R. J. Baxter, *Exactly Solved Models in Statistical Mechanics* (Academic Press, London, 1982).
- ⁴⁸ See, for example, B. M. Ocko, R. J. Birgeneau, and J. D. Litster, Phys. Rev. Lett. **52**, 208 (1984).
- ⁴⁹ D. Stauffer, M. Ferer, and M. Wortis, Phys. Rev. Lett. **29**, 345 (1972).
- ⁵⁰ P. C. Hohenberg, A. Aharony, B. I. Halperin, and E. D. Siggia, Phys. Rev. B **13**, 2986 (1976).
- ⁵¹ D. A. Bruce, J. Phys. C **14**, 5195 (1981).
- ⁵² M. Hagen and D. McK. Paul, J. Phys. **30**, 5605 (1984).
- ⁵³ M. Kardar and A. N. Berker, Phys. Rev. Lett. **48**, 1552 (1982).
- ⁵⁴ D. E. Moncton, P. W. Stephens, R. J. Birgeneau, P. M. Horn, and G. S. Brown, Phys. Rev. Lett. **46**, 1533 (1981).
- ⁵⁵ P. W. Stephens, P. A. Heiney, R. J. Birgeneau, P. M. Horn, D. E. Moncton, and G.S. Brown, Phys. Rev. B **29**, 3512 (1984).
- ⁵⁶ Y. R. Xing, J. P. Zhang, J. A. Wu, C.Z. Liu, and C. H. Wang, Surf. Sci. Lett. **232**, L215 (1990).
- ⁵⁷ Y. Imry and S.-K. Ma, Phys. Rev. Lett. **35**, 1399 (1975).

- ⁵⁸ See, for example, D. Andelman and A. N. Berker, *Phys. Rev. B* **29**, 2630 (1984), and references therein.
- ⁵⁹ R. J. Baxter, *J. Stat. Phys.* **52**, 639 (1988).
- ⁶⁰ G. Albertini, B. M. McCoy, and J. H. H. Perk, *Phys. Lett. A* **135**, 159 (1989).
- ⁶¹ J. L. Cardy, *Nucl. Phys. B* **389**, 577 (1993).
- ⁶² P. A. Heiney, R. J. Birgeneau, G. S. Brown, P. M. Horn, D. E. Moncton, and P. W. Stephens, *Phys. Rev. Lett.* **48**, 104 (1982).
- ⁶³ R. J. Birgeneau, J. Als-Nielsen, and G. Shirane, *Phys. Rev. B* **16**, 280 (1977).